A contact algorithm for smoothed particle hydrodynamics

Article *in* Computer Methods in Applied Mechanics and Engineering · March 2000

DOI: 10.1016/S0045-7825(99)00442-9

3 authors, including:

James Campbell
Brunel University London
66 PUBLICATIONS **1,384** CITATIONS

SEE PROFILE

Rade Vignjevic
Brunel University London
112 PUBLICATIONS **1,889** CITATIONS

SEE PROFILE

ELSEVIER

Comput. Methods Appl. Mech. Engrg. 184 (2000) 49–65

Computer methods in applied mechanics and engineering

www.elsevier.com/locate/cma

A contact algorithm for smoothed particle hydrodynamics

J. Campbell [a], R. Vignjevic [a,*], L. Libersky [b]

[a] *Department of Aerospace Science, College of Aeronautics, Cranfield University, Cranfield, Bedford MK43 0AL, UK*
[b] *Los Alamos National Laboratory, Los Alamos, NM 87545, USA*

Received 28 October 1998

Abstract

This paper describes the development and testing of a contact algorithm for Smoothed Particle Hydrodynamics (SPH). The treatment of contact boundary conditions in SPH has not been adequately addressed, and the development of the normalised smoothing function approach has highlighted the need for correct treatment of boundary conditions. A particle to particle contact algorithm was developed for 2D. The penalty formulation was used to enforce the contact condition, and several equations for the penalty force calculation were considered. The contact algorithm was tested for 1- and 2D problems for the velocity range between 0.2 and 4.0 km/s to determine the best penalty force equation and the best approach for applying the contact force. The tests showed that the zero-energy mode problem in the SPH method had to be addressed, as contact excited a zero-energy mode that caused non-physical motion of particles. The test results were compared to the DYNA3D results for the same problems.

1. Introduction

Smoothed Particle Hydrodynamics (SPH) is a method that offers considerable promise as a numerical method for modelling problems involving large deformations. Originally developed for treating astrophysics problems [1,2], it was first extended to solid mechanics problems by Libersky [3], and was successfully applied to problems such as hypervelocity impact [4]. However the SPH method had several problems, which were detailed in a study by Swegle [5]. These problems were the tensile instability, lack of consistency and zero-energy modes. Swegle and co-workers developed the conservative smoothing approach as a cure for the tensile instability [6]. Johnson developed the normalised smoothing approach to give the method linear consistency [7].

The method improvements in accuracy and stability achieved by kernel re-normalisation or correction have highlighted another problem with SPH, incorrect treatment of boundary conditions. When using the normalised conservation Eqs. (1.1), (1.2), (1.3), (1.4), the free-surface boundary condition is no longer satisfied at boundaries [8], as the kernel normalisation acts as a correction for the lack of neighbours. This results in unphysical behaviour, with stress and shock waves not being reflected from a free surface. Therefore, it is necessary to treat the essential boundary conditions in a rigorous way.

$$\frac{\partial \rho_i}{\partial t} = \rho_i \left[-\sum_j \frac{m_j}{\rho_i \rho_j} \left(v_j^\alpha - v_i^\alpha \right) \frac{\partial W_{ij}}{\partial x^\alpha} \right] B^{\alpha\alpha}, \tag{1.1}$$

* Corresponding author. Tel.: +44-1234-754-736; fax: +44-1234-752-149.
E-mail address: v.rade@cranfield.ac.uk (R. Vignjevic).

0045-7825/00/$ - see front matter
PII: S0045-7825(99)00442-9

$$\frac{\partial v_i^\alpha}{\partial t} = \left[-\sum_j \frac{m_j}{\rho_i \rho_j} \left(\sigma_j^{\alpha\beta} - \sigma_i^{\alpha\beta} \right) \frac{\partial W_{ij}}{\partial x_i^\gamma} \right] B^{\gamma\beta}, \tag{1.2}$$

$$\frac{\partial E_i}{\partial t} = \sigma^{\alpha\beta} \left[-\sum_j \frac{m_j}{\rho_i \rho_j} \left(v_j^\alpha - v_i^\alpha \right) \frac{\partial W_{ij}}{\partial x^\gamma} \right] B^{\gamma\beta}, \tag{1.3}$$

where

$$\left[B^{\gamma\beta} \right] = \left[-\sum_j \frac{m_j}{\rho_j} \left(x_j^\gamma - x_i^\beta \right) \frac{\partial W_{ij}}{\partial x_i^\beta} \right]^{-1}. \tag{1.4}$$

The approximations in SPH do not have the property of strict interpolants so that in general they are not equal to the to the particle value of the dependent variable, i.e. $u^h(x_j) = \sum_I \phi_I(x_j) u_I \neq u_j$. Consequently it does not suffice to zero u_I at the boundary positions to enforce homogeneous boundary conditions.

Campbell [9] suggested an approach for the systematic treatment of boundary conditions by re-considering the original kernel integral estimates and taking into account the boundary conditions through residual terms in the integral by parts. Randles and Libersky [10] were first to propose a more general treatment of the free surface boundary condition based on an extension of the ghost particle method. In this, the boundary was considered to be a surface one half of the local smoothing length away from the so-called boundary particles. A boundary condition was applied to a field variable by assigning the same boundary value of the variable to all ghost particles. A constraint was imposed on a specific boundary by interpolating smoothly between the specified boundary particle value and the calculated values on the interior particles. This served to communicate to the interior particles the effect of the specific boundary condition. This was the approach we adopted for treatment of the free surface boundary condition.

The contact boundary condition has also been successfully ignored in SPH. Contact between two bodies has been handled through the conservation equations, with no restriction on particles from one body being treated as neighbour particles of a particle in another body. They then interact through the sums over neighbour particles. However, when using this method a degree of penetration and mixing occurs at the contact surface as SPH does not require the velocity field to be single valued. Typically the first one to two particle rows of each body pass each other. Monaghan [11] proposed a modification to prevent this penetration, which he called XSPH. While Monaghan's modification does prevent penetration it does nothing to solve two other problems with treating contact through the conservation equations:

- Generation of tensile forces, resisting separation of two bodies.
- Generation of shear stresses preventing friction-less or low friction sliding.

Different contact algorithms have been used with SPH when combining the SPH method with the FE method [12,13], but the only purpose of these algorithms were to allow SPH nodes to interact with an FE mesh.

From a literature survey and our experience in dealing with the contact problem in the finite element method, it was concluded that the penalty method would be a good starting point for contact in SPH due to its simplicity and efficiency.

An advantage of the SPH method is its conceptual simplicity and ease of extension to higher dimensions. In an attempt to preserve these advantages, a particle to particle contact algorithm was developed. This also removed the need to define the material boundary as a line in 2D. In common with the treatment of the free-surface condition, the location of the boundary was fixed at $h/2$. So contact was between spheres of radius $h/2$.

Due to non-uniqueness of the surface normal at vertices it was necessary to calculate two surface normals for each boundary particle, and detect a corner when the angle between the two normals exceeds a specified angle. For a corner particle with no contact the free-surface condition was applied in the directions of both surface normals, for a corner particle with contact the free-surface condition was only applied in the direction of the surface normal not used by the contact algorithm.

Different methods for the penalty force calculation were evaluated in 1D. This included expressions for the contact force based on penetration and penetration velocity. Different penalty force algorithms were evaluated by comparison with contact enforced by including all materials in contact in the kernel sum. The favoured contact force calculation methods were applied to 2D contact algorithms. The treatment of smooth boundary and boundary with vertices as a free-surfaces and in contact was assessed. Few simple illustrative impact problems were analysed to demonstrate accuracy and numerical efficiency of the contact algorithm developed.

SPH results for both 1D and 2D were compared with finite element analyses, made using the DYNA3D code.

2. Contact algorithm

Following the approach proposed by Libersky [10], the boundary was considered to be a surface one half of the local smoothing length away from the boundary SPH particles. Two principal choices for treatment of contact detection and contact force application were considered: particle to surface contact, and particle to particle contact. Fig. 1 shows a 2D example of both cases. The arrows denote the unit normal vector to the particle calculated by the gradient of unity method [10], the dashed lines represent the surfaces used to determine if there is contact.

In the particle to surface case contact is between a circle of radius $h/2$, and a straight line drawn between points that lie $h/2$ along the particle normal vector. If this line intersects the circle then contact has occurred. When contact occurs the restoring force is applied along the normal to the surface, and the force would have to be divided between the two particles at either end of the contact line. This approach is based on the contact algorithms used in Lagrangian finite element codes. As for the finite element algorithms, the reliability of this approach would be improved by making the algorithm symmetric, so that every particle is considered as both a contact particle and a member of a contact surface.

In the particle to particle case, contact is between two circles each of radius $h/2$. Contact occurs when the two circles intersect, which is easily determined by checking the inter-particle distance. In this method only the interaction of two particles is considered at any one time, removing the need to consider each particle twice in the algorithm. This approach has many similarities with Belytschko's pinball contact algorithm [14,15].

The particle to particle approach was selected as it is more in keeping with the meshless approach, and its extension to 3D would not be complex. Extending the particle to surface algorithm to 3D would be complicated by the need to define a boundary surface. Furthermore, this surface needs to be redefined regularly as bodies in contact deform.

In the particle to particle method determination of the contact force vector is an obvious problem. The contact force should be applied in a direction normal to the contact surface, however except in special cases, this results in a force vector that does not pass through the centre of mass of the particles in contact, generating a moment. Applying the contact force along the vector connecting the particle centres solves this

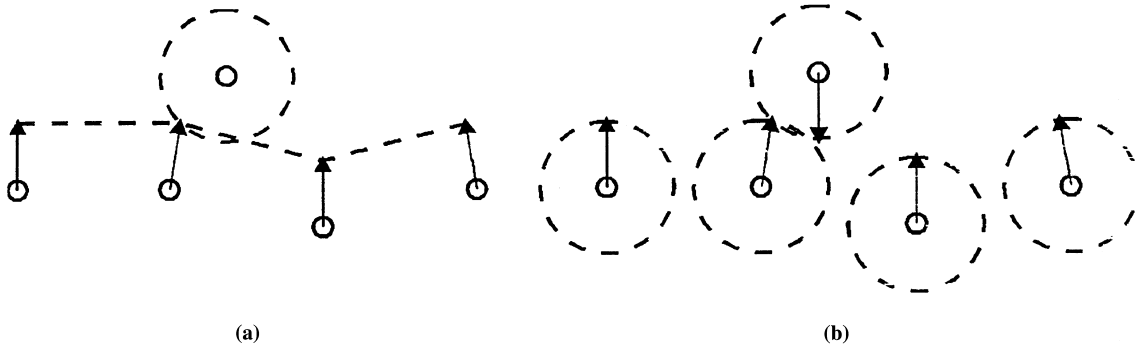

Fig. 1. Principle choices for detection of contact. (a) Particle to surface contact; (b) particle to particle contact.

problem, but the contact force now has a component tangential to the contact surface. Algorithms for both cases were developed, and are described below.

Once contact is detected a method is required to enforce the contact condition. The penalty method was chosen to enforce contact as the simplest and most straightforward method.

2.1. Contact force applied between particle centres

Penalty contact algorithms are based on the assumption that there is certain amount of penetration between the bodies in contact. The contact force is usually function of penetration, penetration rate or both. Thus, penetration calculation is an important part of this type of contact algorithm.

In this simple case, penetration is detected if

$$p = \frac{h_i + h_j}{2} - |r_{ij}| \geqslant 0, \tag{2.1}$$

where $r_{ij} = x_j - x_i$, p the penetration, r_{ij} the vector from the centre of particle i to the centre of particle j and h_i, h_j are smoothing distances for particles i and j, respectively.

The actual penetration is defined by Eq. (2.1). The contact force is applied along vector r_{ij}.

2.2. Contact force applied along average normal

For the stress-free boundary condition the surface normal at each boundary particle has been found, but it is not possible to assume that the normals on the particles in contact are equal and opposite. An estimate to the normal to the contact surface is found by taking the difference between the two unit normal vectors resulting in a vector that when normalised is the average of the two vectors.

This average normal vector is the vector along which the contact force is applied. So the magnitude of the penetration can be defined as the relative displacement of the particles in the direction of the average normal that would result in zero penetration, Eq. (2.2). This is the definition of penetration that is used in the pinball algorithm [14].

$$p = \sqrt{d^2 - r_{ij}^2 + \left(n_{\text{av}} \cdot r_{ij}\right)^2} - \left(n_{\text{av}} \cdot r_{ij}\right), \tag{2.2}$$

where $d = (h_i + h_j)/2$ and n_{av} is the average normal vector.

2.3. Enforcing the contact condition

The use of the particle to particle approach means that penetration is detected only when the distance between the two particles is $< 0.5(h_i + h_j)$. If the two particles completely pass each other then penetration is no longer detected, and no contact force is applied. Preventing this from happening places a lower limit on the magnitude of the penalty force.

Three different expressions for the penalty force were investigated, and implemented into the code. This allowed the sensitivity of the contact algorithm to the contact force type to be tested.

The first contact force considered was the force used by Belytschko in the pinball algorithm, see [15] for details. This defines the contact (penalty) force as

$$F = K_p \min(F_1, F_2), \tag{2.3}$$

where

$$F_1 = \begin{cases} \dfrac{\rho_i \rho_j R_i^3 R_j^3}{\rho_i R_i^3 + \rho_j R_j^3} \cdot \dfrac{\dot{p}}{\Delta t}, & \dot{p} > 0, \\ 0, & \dot{p} < 0, \end{cases} \tag{2.4}$$

$$F_2 = \left[\frac{G_i G_j}{G_i + G_j} \sqrt{\frac{R_i R_j}{R_i + R_j}} \right] p^{3/2}, \tag{2.5}$$

where ρ_i and ρ_j are the densities of the two particles, G_i and G_j the shear moduli, R_i and R_j are the radii, K_p is a scale factor.

Eq. (2.4) is derived by considering the force required to bring the two particles to rest with respect to each other, while conserving momentum, in an ideal plastic collision. Eq. (2.5) is derived from the equations for contact force between two solid elastic spheres.

The second contact force considered, referred to in this paper as type 2, Considered was

$$F = K_p \begin{cases} \max(F_1, F_2), & \dot{p} > 0, \\ 0, & \dot{p} < 0, \end{cases} \tag{2.6}$$

where K_p is a scale factor,

$$F_1 = \frac{mp}{\Delta t^2}, \tag{2.7}$$

$$F_1 = \frac{2mcp}{\Delta t \Delta x}, \tag{2.8}$$

$$\Delta x = \left| x_j - x_i \right|.$$

Eq. (2.7) is used by Swegle [5] for contact between SPH nodes and finite elements. It is derived by assuming that the rate of penetration can be defined as $p/\Delta t$ and applying a force sufficient to bring the node penetrating the finite element mesh to rest over a single time step. Eq. (2.8) can be derived by assuming that $m_i = m_j = m$ and applying a force sufficient to bring to rest a body of mass 2 m travelling at the relative velocity of the two particles, v':

$$F = \frac{2mv'}{\Delta t}. \tag{2.9}$$

Then substituting $v' = cp/\Delta x$, where $\Delta x/c$ is an approximation to the time over which the penetration has occurred, gives (2.5).

The equation $\sigma = \rho c v$ for the stress behind a 1D elastic wave is equivalent to (2.5) if the following substitutions are made: $\sigma = F/A$ and $v = p/\Delta t$.

The third contact force, referred to in this paper as type 3, considered was

$$F = \begin{cases} \dfrac{\left| v_j - v_i \right|}{\frac{\Delta t}{m_i} + \frac{\Delta t}{m_j}}, & \dot{p} > 0, \\ 0, & \dot{p} < 0. \end{cases} \tag{2.10}$$

This was derived, by considering the force required to bring the two particles to rest with respect to each other, while conserving momentum, in an ideal plastic collision. The contact force in one time step applies the same impulse to both contact particles

$$F\Delta t = m_i \Delta v_i, \qquad F\Delta t = m_j \Delta v_j. \tag{2.11}$$

If the particles are to be brought to rest with respect to each other, then the rate of change of penetration has to be, $\dot{p} = \Delta v_i + \Delta v_j$, which using Eq. (2.11) yields

$$\dot{p} = \frac{F_1 \Delta t}{m_i} + \frac{F_1 \Delta t}{m_j}. \tag{2.12}$$

Substituting the relative velocity $|v_j - v_i|$ for $\dot{p}$ in Eq. (2.12) results in the third contact force expression. No scale factor or other correction term is required for this type of contact force.

2.4. Linking free surface condition with contact

The contact algorithm should allow surfaces to come together and separate in a natural manner. This requires the stress free boundary condition algorithm to be modified so that this boundary condition is not applied to boundary particles in contact.

3. 1D tests

The first set of tests was in 1D. The aim of these was to test the effects of the different contact (penalty) force algorithms, in exclusion from any effect that could occur in 2D from the two different methods of calculation of the vector along which the contact force was applied.

The test problem used was a symmetrical impact of two 0.4 cm long steel bars, Fig. 2. 100 particles were placed along the 1D line, 50 particles in each bar. The smoothing length was 0.008 cm and the initial inter-particle space was equal to the smoothing length. The space between the two contact particles was 0.01 cm, so there was no initial penetration. Each bar was given an equal but opposite initial velocity of 2 km/s.

To provide a reference point the problem was initially run with no contact, using kernel sums to allow interaction between the two bodies. With the kernel sums the two end particles were initially in contact as the distance between the two was 1.25 h. Fig. 3 shows the resulting stress profiles, compared with finite element results for the same problem using the DYNA3D code. At time 0.2 μs the shock waves are propagating away from the point of contact. The value of k, time step scale factor, used for the results shown was $k = 0.5$. The problem was also run with a value of $k = 1.5$ with no problems, the only difference observed was a higher amplitude, by a factor of 3–4, in the stress oscillations behind the shock wave. With this reference point established, runs were made to compare the different contact force types. Both the type 1 and the type 2 contact forces resulted in similar overall behaviour, therefore results are presented for the contact force types 2 and 3 only. Fig. 4 shows the stress profile at time 0.2 for force types 2 and 3, with the stress profile for kernel contact shown for comparison. Fig. 5 shows the stress profile at time 0.7 for force types 2 and 3, with the stress profile for kernel contact shown for comparison.

In Figs. 4 and 5 considerable oscillation can be seen in the stress at the interface for both cases. A sensitivity analysis was performed in which the contact force scale factor K_p was varied between 0.008 and 0.2 for contact force type 2. Best results were obtained for $K_p = 0.05$, the amplitude of the spurious stress oscillations was significantly reduced.

This oscillation was described by Swegle [5] who observed it when modelling the 1D impact of two initially separated bodies using kernel contact. This oscillation corresponds to a zero energy mode, for which stress field does not cause particle accelerations that would reduce the stress amplitude. Swegle showed that this was a characteristic of the SPH method, as the SPH estimate to the stress field has its local maxima and mimima at the particles giving the stress field gradient of zero. In the SPH method no acceleration will be produced at a particle if the stress at the two neighbour particles is equal, this is independent of the stress at the particle itself. This is the stress version of the SPH zero-energy mode where an

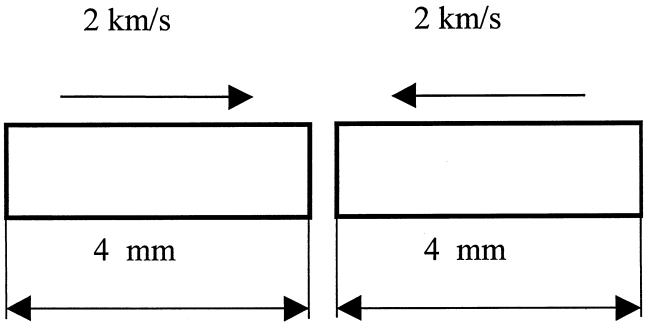

Fig. 2. Schematic representation of the 1D test problem.

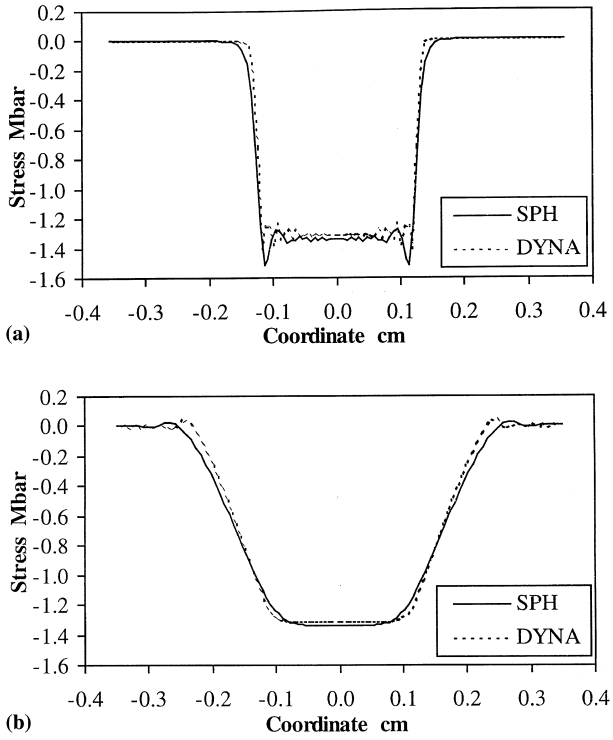

Fig. 3. Comparison of SPH and finite element stress profiles. (a) Time 0.2 μs; (b) time 0.7 μs.

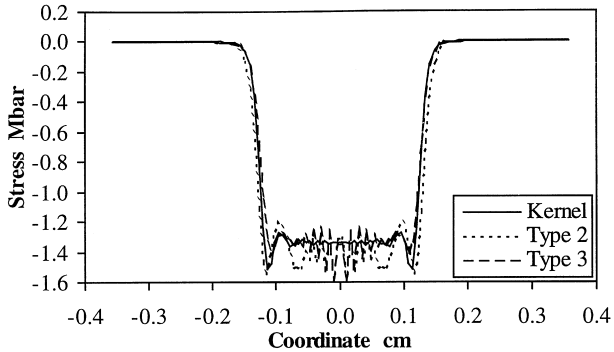

Fig. 4. Stress profiles at 0.2 μs for kernel contact, contact force types 2 and 3. Contact force scale factor for the contact force type 2 was $K_p = 0.05$. Time step scale factor was $k = 0.5$. Impact velocity 2 km/s.

alternating velocity field does not generate stresses in the material to resist the particle motion. Swegle attempted to control the oscillation by varying the time step, the artificial viscosity coefficient and the smoothing length, all without success.

The contact algorithm, using the third type of contact force, showed the best agreement with the velocity profile seen with kernel contact. However, the stress profiles showed that the stress oscillation was also present with this contact force type.

The stress oscillation in the region of the contact did not change significantly during contact. Fig. 6 compares the stress profile near the contact surface between time 0.2 and 0.7 μs. This showed that only a small decrease in the amplitude of stress oscillation has occurred.

If the spurious stress oscillation did not have any affect on the results of the calculation then it would have been possible to ignore it. During the early stages of the calculations, as have been discussed so far, it

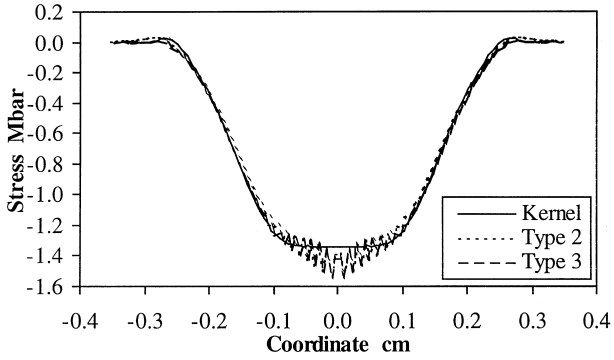

Fig. 5. Stress profiles at 0.7 μs for kernel contact, contact force types 2 and 3. Contact force scale factor for the contact force type 2 was $K_p = 0.05$. Time step scale factor was $k = 0.5$. Impact velocity 2 km/s.

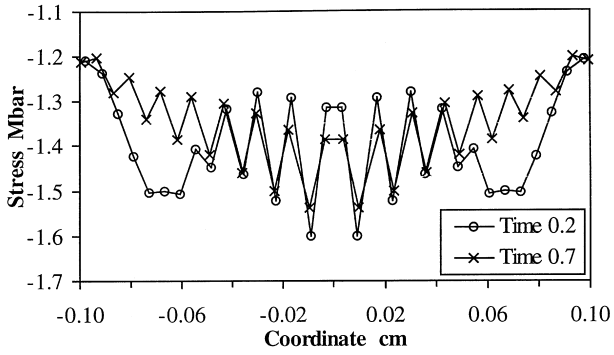

Fig. 6. Detail of stress oscillation at contact surface, contact type 2.

was not significant. It was found that it can have a significant effect once the release waves arrive at the contact surface. The spurious stress oscillation caused high tensile stresses in the material, when the release waves reach the contact interface by affecting the behaviour of the nodes in contact. The root cause of this tensile stress was the incorrect behaviour of the boundary particles due to the spurious stress oscillations. This can be explained by considering the momentum equation.

In 1D, considering only the nearest neighbours, the momentum equation for an internal particle reduces to

$$\frac{\mathrm{d}v_i}{dt} = \left[-\left(\frac{m_{j1}}{\rho_{j1}} (\sigma_{j1} - \sigma_i) \frac{\mathrm{d}W_{ij1}}{\mathrm{d}x} \right) - \left(\frac{m_{j2}}{\rho_{j2}} (\sigma_{j2} - \sigma_i) \frac{\mathrm{d}W_{ij2}}{dx} \right) \right], \tag{3.1}$$

where $j1$ and $j2$ are the two neighbour particles. So when $\sigma_{j1} = \sigma_{j2}$ the acceleration is zero. For a boundary particle this equation is

$$\frac{\mathrm{d}v_i}{\mathrm{d}t} = \left[-\frac{m_j}{\rho_j} (\sigma_j - \sigma_i) \frac{\mathrm{d}W_{ij}}{\mathrm{d}x} \right] B \tag{3.2}$$

as the stress oscillation causes $\sigma_j \neq \sigma_i$ then the boundary particle has a non-zero acceleration. In all cases the stress oscillation caused by contact had $\sigma_j > \sigma_i$, which causes the boundary particle to have an acceleration away from its neighbour particle.

In most cases the effect that the tensile stress had on the final result was to delay the separation of the two bars, and to generate a tensile stress wave that propagated through the material. In one case the stress was high enough to cause numerical fracture, splitting the particles near the contact point from the remainder, Fig. 7.

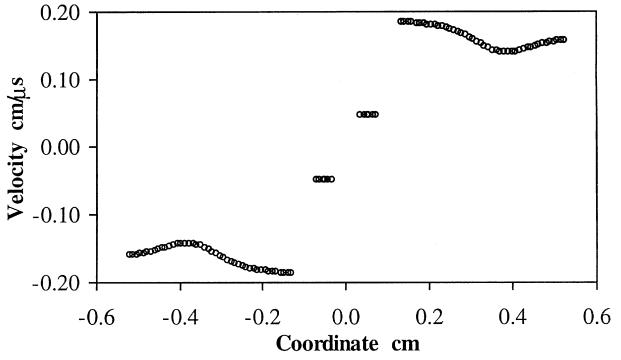

Fig. 7. Velocity profile at 2.0 μs. Tensile stresses have caused numerical fracture near contact point. Penalty type 2, $k = 0.5$, $K_p = 0.01$. Impact velocity 4.0 km/s.

The effect of the spurious stress oscillation has been established. As it had significant effect on the results it needed to be controlled. Tests were performed to find the effect of varying the time step, contact force and initial material velocity on the oscillation. Fig. 8 compares the stress profile at 0.2 μs for a $k = 0.5$ and $k = 0.1$. Both use penalty type 2 with $K_p = 0.05$. Reducing the time step has only reduced the extent of the oscillation, from 10 particles to 8 particles, it has not reduced the amplitude.

The amplitude of the oscillation was most sensitive to the magnitude of the contact force. Reducing the contact force gave a significant reduction in the amplitude. Fig. 9 compares the stress profile at 0.2 μs for $k = 0.5$, $K_p = 0.05$ and $k = 0.1, K_p = 0.01$. Reducing the contact force has reduced the amplitude of the oscillations.

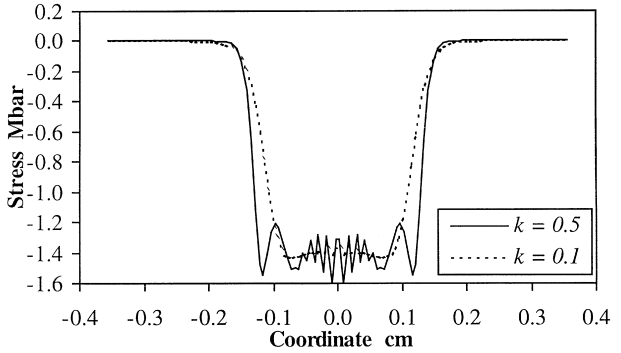

Fig. 8. Stress profiles at 0.2 μs for $k = 0.5$ and $k = 0.1$. showing the effect on the stress oscillation of reducing the time step. $K_p = 0.05$. Impact velocity 4.0 km/s.

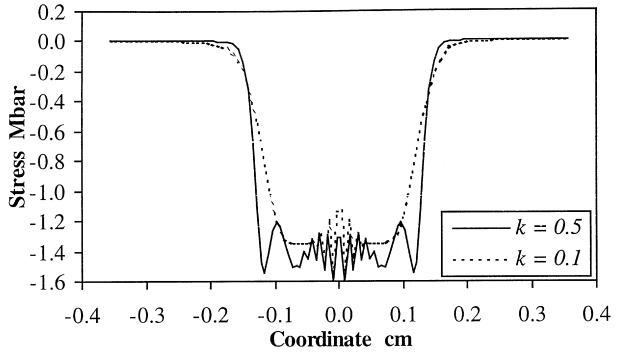

Fig. 9. Stress profiles at 0.2 μs for $k = 0.5$, $K_p = 0.05$ and $k = 0.1$, $K_p = 0.01$. showing the effect on the stress oscillation of reducing the contact force scale factor. Impact velocity 4.0 km/s.

Reducing the impact velocity, which also has the effect of reducing the contact force, also reduced the stress oscillation. At the higher velocities the contact force can not be reduced to a level that controls the oscillation, as a low contact force leads to a large penetration which causes the contact algorithm to break down. Reducing the time step and the contact force gave a significantly reduced amplitude, and offered a way of controlling the amplitude of oscillating stress component. The disadvantage of this was that the tests with a reduced time step were using a time step of 5% of the maximum stable value. In higher dimensions with the consequent larger numbers of particles this size of time step would increase the computational cost of the calculation by an order of magnitude over the cost when using the kernel to provide contact.

4. 2D tests

As the 1D tests showed that the behaviour of penalty force types 1 and 2 were similar, only penalty force types 2 and 3 were used in the 2D tests. The contact algorithm was tested in 2D by modelling the normal symmetrical impact of two steel blocks. Each block was 10 mm × 4 mm and consisted of 50 particles by 20 particles, giving a total of 2000 particles in the whole model. The two block's initial relative velocity was 0.2 to 4.0 km/s, see Fig. 10. The contact boundary particles in each body were initially spaced h apart, so the initial penetration was zero.

The problem was first analysed using DYNA3D in order to provide results for comparison, the DYNA results are shown in Fig. 11.

Initial test results showed that the contact algorithm required improvement in its treatment of corner particles. When the stress free boundary condition was not applied to the corner particles in contact, this caused incorrect behaviour at the corner particles at either end of the contact surface. As the stress free condition was not applied release waves were not generated correctly at the corner particles. The result was that the horizontal velocity of the corner particles was too low, Fig. 12a. Applying the stress free boundary condition to the corner particles corrected this, but resulted in significant inter-penetration of the corner particles, Fig. 12b.

In order to treat the corner particles correctly two surface normal vectors were required. If the corner particle was not in contact then the stress free boundary condition was applied for both particle normals. If the particle was in contact then the stress free boundary condition was only applied in the direction of the free surface particle normal. This allowed for the correct behaviour of the corner particles.

For contact it was necessary to find the best normal to use. The best normal was defined as the normal, which gives the maximum value of the dot product $n \cdot r_{ij}$. Where r_{ij} is the vector between the centres of the two particles in contact and n is the unit normal vector. The best normal was then used for the contact algorithm as if it were the single particle normal. The stress free boundary condition was not applied for that surface normal used in contact. For contact boundary particles that lie on a flat or near flat boundary it was necessary not to apply the stress free boundary condition. To differentiate between a corner particle

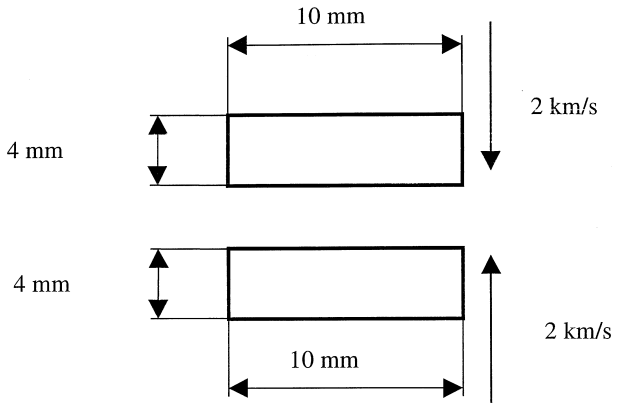

Fig. 10. Schematic representation of the 2D test problem.

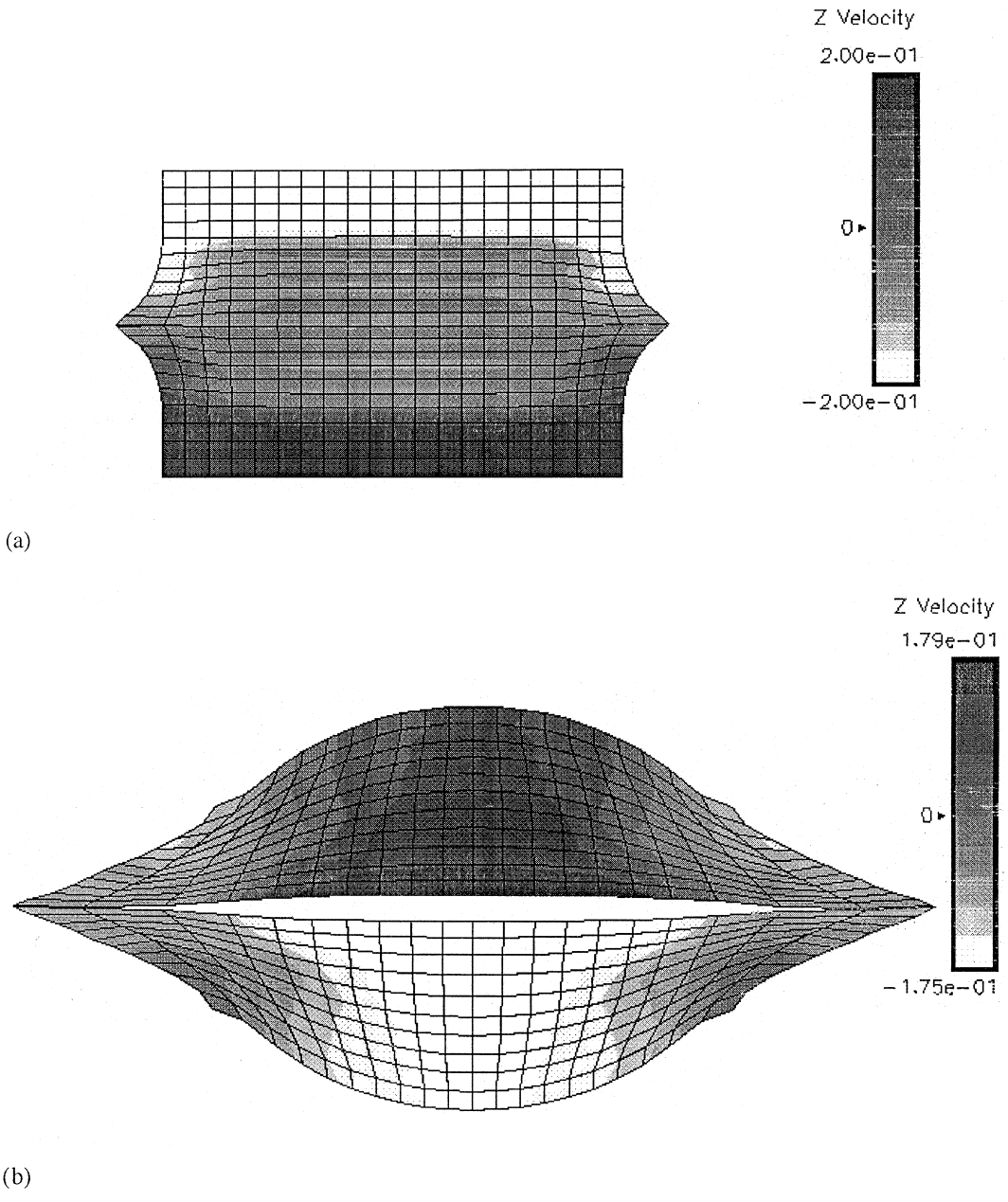

Fig. 11. DYNA results for 2D test problem, contours of z (vertical) velocity. (a) Time 0.04 μs; (b) time 1.4 μs.

and a surface particle the angle between the two normal vectors was calculated. If this angle exceeded a set value then the particle was considered to be a corner particle and both contact and free surface boundary conditions were applied in the directions of corresponding normals. The set value used in the tests was 45°.

The aim of the 2D tests described below was to compare the effects of applying the restoring force along an average particle normal, or along the vector between the two particle centres.

The following four basic cases were considered:

(a) Average normal contact with penalty force type 2.
(b) Average normal contact with penalty force type 3.
(c) Between centres contact with penalty force type 2.
(d) Between centres contact with penalty force type 3.

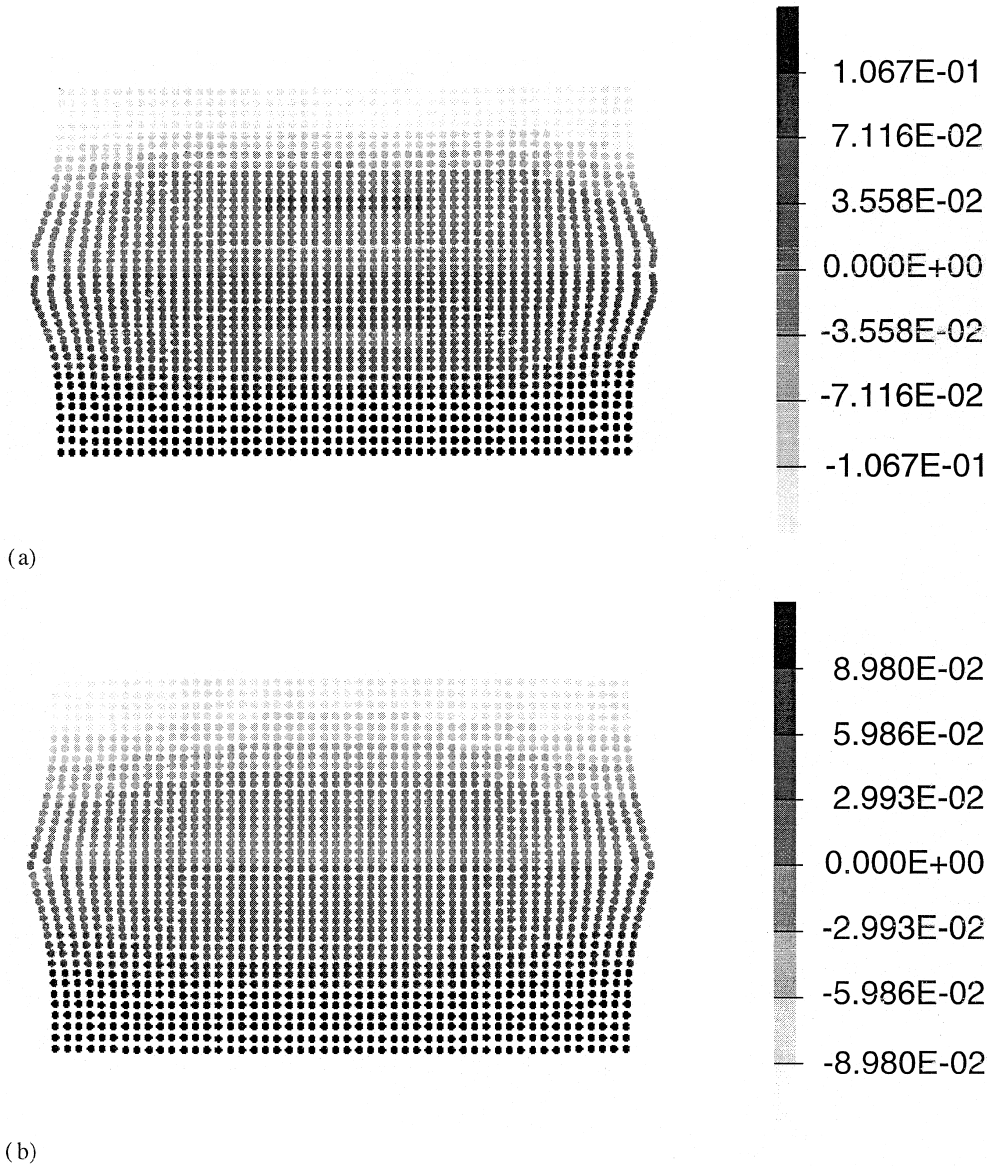

Fig. 12. z velocity at 0.4 μs. One normal vector calculated for each boundary particle. (a) Corner particles do not have stress free condition applied; (b) corner particles have stress free condition applied.

For all four runs k was 0.1, and for penalty force type 2 K_p was 0.05. All four sets of results were very similar so results are shown for case (b), with the corner particles behaving correctly, and the two bodies separating later in the calculation, Fig. 13. In all of these cases the particles in the two bodies were initially aligned, so that there was no difference between the average normal vector and the vector between the particle centres.

To test for the difference between the two methods, the lower block was given an initial horizontal, along the x axis, offset of 0.25 h. This offset causes the two vectors to no longer be aligned, while not allowing a contact particle to be in contact with more than one other contact particle during the early stages of the calculation. To measure the difference between the cases, the total x momentum of each of the two blocks was recorded. To reduce the effect of the offset at the corners, a lower initial relative velocity of 200 m/s was used. Initially the x momentum in each body was zero and in the ideal case it would have remained zero throughout the run. The x momentum time histories for the four cases are shown in Fig. 14.

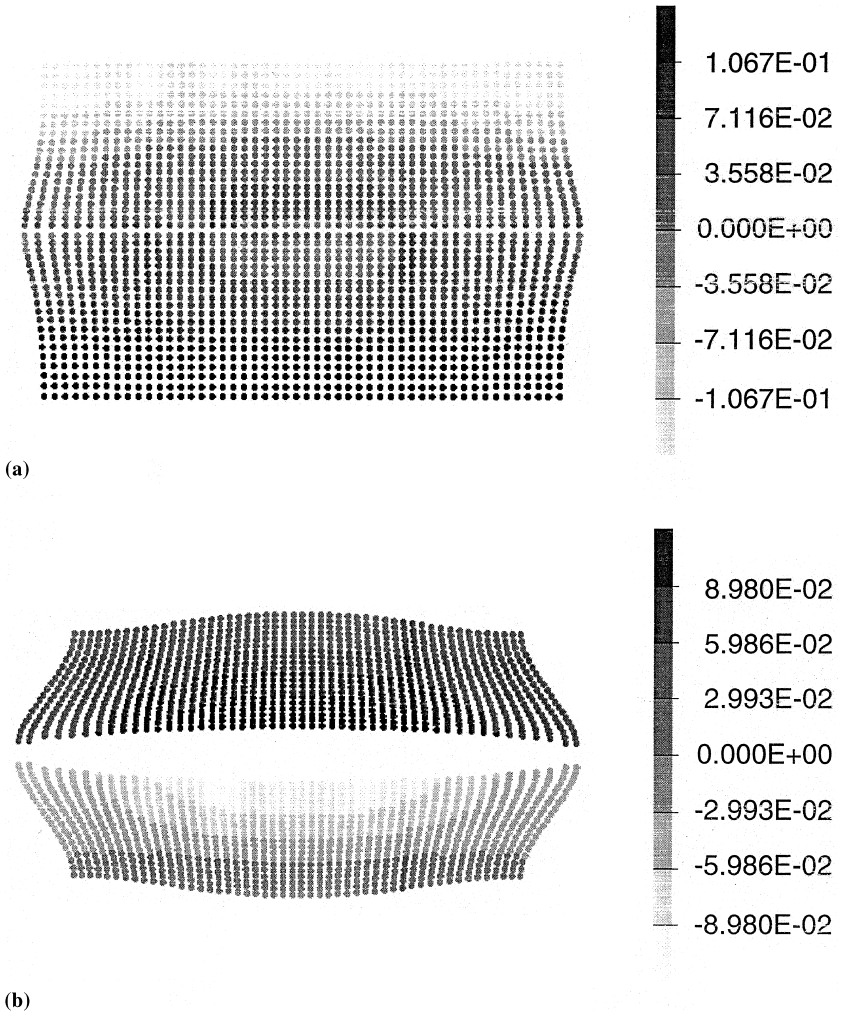

Fig. 13. Verticle velocity for average normal contact, contact force type 3, $k = 0.1$. Impact velocity 4 km/s. (a) Time 0.4 μs; (b) time 1.8 μs.

The difference between the two force vectors was clearly seen. With both penalty force types the between centres algorithm has resulted in a higher x momentum in the two bodies.

	Maximum momentum x
Average normal contact, penalty type 2	3.79×10^{-4}
Between centres contact, penalty type 2	4.30×10^{-3}
Average normal contact, penalty type 3	3.63×10^{-4}
Between centres contact, penalty type 3	5.04×10^{-3}

The maximum value for the average normal contact was at time 0.98 μs, the larger value that occurred later will be commented on shortly. There was an order of magnitude difference between the two cases, but was this difference significant? Each block was 1 cm × 0.4 cm, and the initial material density was 7.89 g/cm^3, giving each block a total mass of 3.156 g. An x momentum of 5.04×10^{-3} is equivalent to an average horizontal velocity for the block of 0.0016 cm/μs, 16% of the initial vertical velocity of the block.

Applying the penalty force along the vector between the two centres has resulted in each block gaining a significant horizontal momentum. These figures are the maximum values. In all cases the momentum drops after reaching its maximum value. This is because the horizontal motion has resulted in a given contact

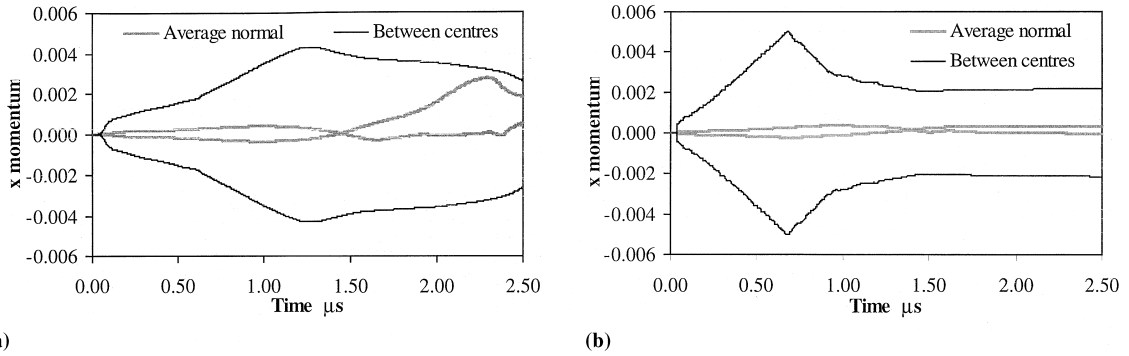

Fig. 14. x momentum time histories for the different force vectors. Impact velocity 200 m/s. (a) Contact force type 2; (b) contact force type 3.

particle coming into contact with the neighbour of its initial contact particle, the resulting penalty force has an x component of opposite sign to the force from contact with the initial particle. By doubling the number of particles in the model the maximum value of the x momentum was reduced ten times.

These tests represent a worst case, where the particle spacing of the two contact surfaces were the same, and all particles were offset in the same direction. In practice it is most likely that the particle spacing of both surfaces would not be identical, and so any forces tangent to the contact surface would not have such a significant global effect.

The momentum time history for the average normal contact with contact force type 2 showed a large change in momentum after 1.5 μs. The cause of this change was an instability that developed near both ends of the contact surface. This instability caused visible, non-physical, particle motions. These motions were largest in this case, but were also visible in the other normal contact case and the between centres with contact force type 2. The only case where visible particle motion was not seen was for the between centres with contact force type 3. Fig. 15 shows the particle x velocities at 2.4 μs for the best and worst cases.

This instability was related to the saw-tooth stress oscillation observed in the 1D tests, as the stress oscillation occurs near the corners before the particle motions become significant. Fig. 16 shows the σ_{xx} stress profile at 1.0 μs of the contact boundary particles of the upper block, for the average normal with contact force type 2. The stress oscillation was pronounced at the two ends of the contact surface. No stress oscillation was observed in the σ_{zz} stress. The stress oscillation was also present in the two other cases where the instability caused visible particle motion.

Examining the particle stresses for the four runs without an initial particle offset showed that the stress oscillation was also present in those results. The instability was also present in 200 m/s impact velocity tests. Like the offset results, the average normal contact with contact force type 2 showed the most extensive instability. Fig. 17 shows plots of the σ_{xx} and σ_{zz} stress components at 1.0 μs for the 4 km/s, average normal case. Well developed instabilities and related errors in the stress distribution can be seen at either end of the contact surface for both stress components.

The presence of the instability appeared to be related to the spurious stress oscillation. The 1D tests showed that reducing the time step scale factor and the penalty force reduced the amplitude and extent of the stress oscillation. Also reducing the impact velocity, with the corresponding decrease in the contact force, reduced the oscillation. Tests were carried out in 2D to find whether this instability is sensitive to the same factors.

The first four tests mentioned in this section, for 4 km/s impact and $k = 0.1$ did not show any visible evidence of the instability. These four tests were repeated with $k = 0.3$, and all four calculations developed the instability. The instability caused visible particle motions by 0.4 μs.

The instability was closely related to the stress oscillation as it occurs in locations where the stress oscillation was already present. The severity of the instability is reduced in the same way as the severity of the stress oscillation reducing time step and contact force. The contact algorithm used had a strong effect on the instability, with the instability being most apparent when applying the contact force along the average normal vector, and least apparent when applying the contact force between the particle centres. The

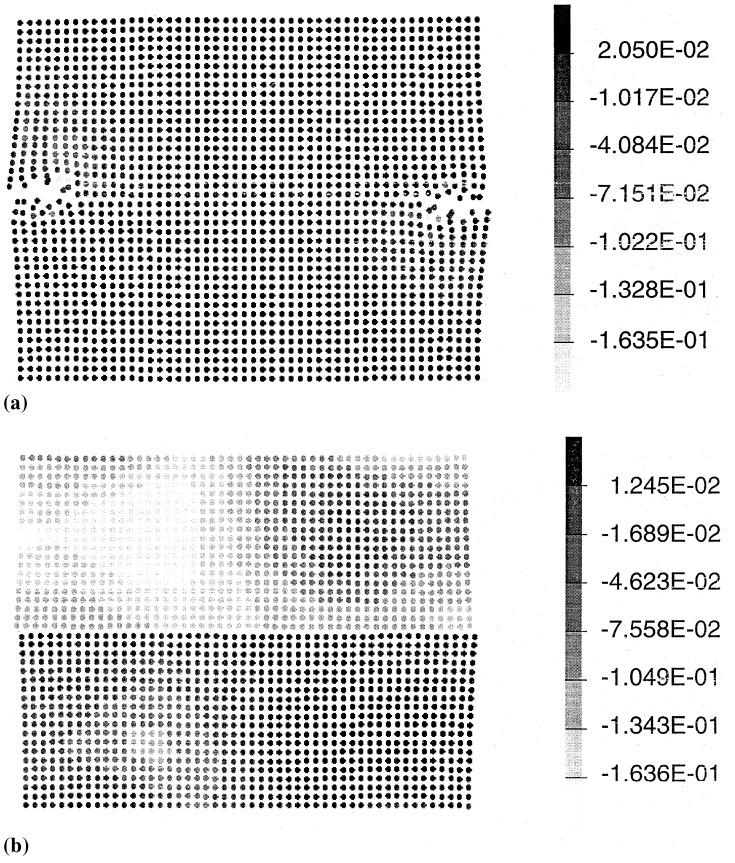

Fig. 15. x velocity at 2.4 μs for offset impact tests. An instability can be seen with the average normal contact case, $k = 0.1$. (a) Average normal contact, contact force type 2; (b) between centres contact, contact force type 3.

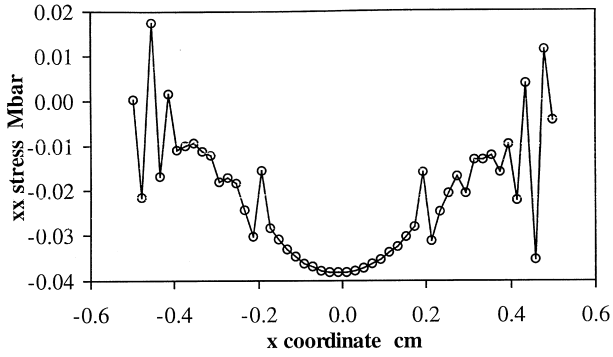

Fig. 16. σ_{xx} profile along contact surface at 1.0 μs for the average normal with contact force type 2, with initially offset particles.

average normal was calculated from the particle normals, which were in turn calculated form the surface geometry of the body. This makes this algorithm sensitive to small changes in the surface geometry.

Further tests are required before a solid conclusion can be drawn as to whether applying the contact force between the particle centres or along an average normal is better. These tests are complicated by the presence of the instability, as over a large range of initial conditions this instability will grow to a point where it prevents the calculation from reaching the termination time or has a significant effect on the global behaviour of the problem. The instability problem must be addressed before further development of the contact algorithms can be carried out.

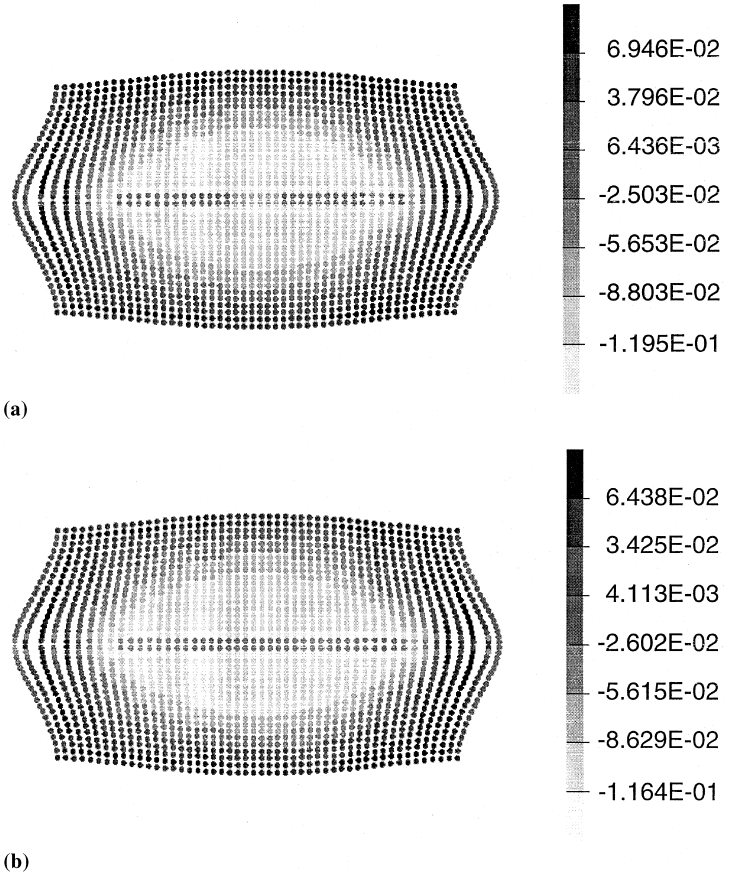

Fig. 17. Stress components at 1.0 μs for average normal contact. $k = 0{:}1$. Instabilities at either end of the contact surface. Impact velocity 4 km/s. (a) σ_{xx} stress component (horizontal); (b) σ_{xx} stress component (vertical).

5. Conclusions

A penalty method for contact in SPH has been developed. The method retained the conceptual simplicity of the SPH method by considering only particle–particle contact. Impact and separation in the velocity range between 0.2 and 4 km/s were successfully modelled. The results were compared to the result from a DYNA3D analysis for the same problem. The difference in stresses and velocities between the best SPH and FE analyses was within 5% for the response time considered.

- Contact excites a stress oscillation in the region of the contact interface. In both 1D and 2D the oscillation resulted in non-physical motion of particles, in some cases rendering the final results completely inaccurate.
- Reducing the time step and contact force significantly reduced the severity of the spurious stress oscillation. The time step required was under 10% of the time step when using kernel contact.
- The stress oscillation is a characteristic of the SPH method, not the particular contact algorithm.
- The presence of the instability prevented the full testing of the proposed contact algorithm.
- The spurious stress oscillation requires (zero energy mode problem) addressing and controlling.

References

[1] R.A. Gingold, J.J. Monaghan, Smoothed particle hydrodynamics: theory and application to non-spherical stars, Mon. Not. R. Astron. Soc. 181 (1977) 375–389.
[2] L.B. Lucy, A numerical approach to the testing of the fission hypothesis, Astronom. J. 82 (1977) 1013–1024.

[3] L.D. Libersky, A.G. Petschek, Smooth particle hydrodynamics with strength of materials, in: H.E. Trease, M.J. Fritts, W.P. Crowley (Eds.), Advances in the Free-Lagrange Method, Springer, New York, 1991, pp. 248–257.
[4] L.D. Libersky, A.G. Petschek, T.C. Carney, J.R. Hipp, F.A. Allahdadi, High strain Lagrangian hydrodynamics, J. Comput. Phys. 109 (1993) 67–75.
[5] J.W. Swegle, S.W. Attaway, M.W. Heinstein, F.J. Mello, D.L. Hicks, An analysis of smoothed particle hydrodynamics. Sandia Report, SAND93-2513, March 1994.
[6] Y. Wen, D.L. Hicks, J.W. Swegle, Stabilising S.P.H. with conservative smoothing, Sandia Report SAND94-1932, August 1994.
[7] G.R. Johnson, R.A. Stryk, S.R. Beissel, SPH for high velocity impact computations, Comput. Methods Appl. Mech. Engrg. 139 (1996) 347–373.
[8] P.W. Randles, L.D. Libersky, Private communication, October 1997.
[9] P.M. Campbell, Some new algorithms for boundary value problems in smooth particle hydrodynamics, Report DNA-TR-88-286, June 1989.
[10] P.W. Randles, L.D. Libersky, Smoothed particle hydrodynamics: some recent improvements and applications, Comput. Methods Appl. Mech. Engrg. 139 (1996) 375–408.
[11] J.J. Monaghan, On the problem of penetration in particle methods, J. Comput. Phys. 82 (1989) 1–15.
[12] G.R. Johnson, Linking of Lagrangian particle methods to standard finite element methods for high velocity impact computations, Nucl. Engrg. Des. 150 (1994) 265–274.
[13] S.W. Attaway, M.W. Heinstein, J.W. Swegle, Coupling of smooth particle hydrodynamics with the finite element method, Nucl. Engrg. Des. 150 (1994) 199–205.
[14] T. Belytscko, M. Neal, Contact-impact by the pinball algorithm with penalty and Lagrangian methods, Int. J. Numer. Methods Engrg. 31 (1991) 547–572.
[15] T. Belytschko, I. Yeh, The splitting pinball method for contact-impact problems, Comput. Methods Appl. Mech. Engrg. 105 (1993) 375–393.